Nanoscale ice-type structural fluctuation in spinel titanates

S. Torigoe, T. Hattori, K. Kodama, T. Honda, H. Sagayama, K. Ikeda, T. Otomo, H. Nitani, H. Abe, H. Murakawa, H. Sakai, and N. Hanasaki

Phys. Rev. B **98**, 134443 — Published 24 October 2018

DOI: 10.1103/PhysRevB.98.134443

Nanoscale Ice-type Structural Fluctuation in Spinel Titanates

S. Torigoe and T. Hattori

Department of Physics, Osaka University, Toyonaka, Osaka 560-0043, Japan

K. Kodama

Material Science Research Center, Japan Atomic Energy Agency, Tokai, Ibaraki 319-1195, Japan

T. Honda, H. Sagayama, K. Ikeda, T. Otomo, H. Nitani, and H. Abe

Institute of Materials Structure Science, High Energy Accelerator Research Organization (KEK), Tsukuba, Ibaraki 305-0801, Japan

H. Murakawa

Department of Physics, Osaka University, Toyonaka, Osaka 560-0043, Japan

H. Sakai

Department of Physics, Osaka University, Toyonaka, Osaka 560-0043, Japan and PRESTO, Japan Science and Technology Agency, Kawaguchi, Saitama 332-0012, Japan

N. Hanasaki*

Department of Physics, Osaka University, Toyonaka, Osaka, 560-0043, Japan

Abstract

In the spinel titanate $MgTi_2O_4$, the tetragonal phase collapses upon substitution of a tiny amount of Mg ions at the Ti site, and the cubic phase with the geometrical frustration is resurrected. The atomic pair distribution function (PDF) and the extended x-ray absorption fine structure (EXAFS) reveal the nanoscale structural fluctuation, in which the Ti atomic displacement has the two-in two-out configuration in the cubic phase. We argue that the geometrical frustration plays an essential role in the collapse of the tetragonal phase and the resultant nanoscale ice-type structural fluctuation.

I. INTRODUCTION

Geometrical frustration is one of central research topics in condensed matter physics, and gives rise to various interesting physical properties originating from the degeneracy. The first example of a frustrated system was crystalline ice and was reported by Pauling [1]. The ice rule, in which the oxygen is coordinated to two covalently-bonded hydrogens and two hydrogen-bonded hydrogens, leads to the disorder state of the hydrogen atoms [2, 3]. Anderson applied this ice-rule concept to the spin and charge degrees of freedom in the corner-sharing tetrahedral lattice, as shown in Fig.1(a) [4]. The spin-ice state, in which the spin has the two-in two-out type local order, was found in the pyrochlore titanates [5].

In order to pursue the ice physics, it is important to realize the structural ice-type state in the condensed matter, especially the strongly correlated electron systems, which have high controllability and many degrees of freedom. The structural ice-type state, that is, the "displacement-type ice" is defined so that two atoms are displaced inward and the other two atoms are displaced outward in the tetrahedra in the pyrochlore lattice. Figure 1(b) illustrates the original positions (blue) and the displaced positions (green) of atoms. Here, the lengths of the red, grey, and blue bonds become short, intermediate, and long, respectively.

In the d^n electronic system, for example, the spinel compounds $CuIr_2S_4$ and AlV_2O_4, in which the B sites form the pyrochlore lattice, exhibit nontrivial ground states forming the structural multimer to relieve the frustration [6–10], since n valence electrons tend to create several covalent bonds within the multimer. On the other hand, in the quantum spin-type d^1 electronic system, one valence electron can create a spin-singlet pair and a single bond. This spin-lattice coupling can be a driving force for realizing the structural two-in state in the pyrochlore lattice. Thus, we focused on the spinel titanate $MgTi_2O_4$ (Ti^{3+} $(3d)^1$ $S = \frac{1}{2}$), and explored for the displacement-type ice.

In $MgTi_2O_4$, the crystal field given by the oxygen octahedron splits the orbitals into the e_g and the t_{2g} orbitals in the Ti ions, and one electron exists in the latter degenerate orbitals. The structural transition from the cubic phase (space group $Fd\bar{3}m$) to the tetragonal phase ($P4_12_12$) occurs upon cooling at $T_c \approx 260\,\mathrm{K}$ [11]. Below T_c, the long and the short bonds between the Ti ions are arranged alternately along the c axis, is formed [12]. The Ti atomic displacement follows the ice rule. However, since the long-range structural order grows below T_c, the frustration is relieved. As a potential origin of this structural transition, the

Peierls mechanism was proposed [13]. The structural transition creates the Peierls gap in the bands consisting of the d_{yz} and d_{zx} orbitals. Another potential mechanism was a valence-bond model suggesting a group of spin-singlet dimers with a degeneracy [14–16]. Isobe *et al.* reported a decrease in the magnetic susceptibility below T_c for $x=0$, and ascribed this reduction to the spin singlet [11]. In Mg-substituted $Mg_{1+x}Ti_{2-x}O_4$, the decrease of the magnetic susceptibility is reduced [17, 18].

In this study, in order to explore the structural ice-type state, we substituted the non-magnetic Mg ions for Ti ions in $MgTi_2O_4$, and shortened the correlation length of the tetragonal structure. For its detection, we measured the two-body correlation with Ti ions in $Mg_{1+x}Ti_{2-x}O_4$ by the neutron atomic pair distribution function (PDF) and the extended x-ray absorption fine structure (EXAFS). By performing the nanoscale structural analyses, we found the nanoscale ice-type structural fluctuation in the cubic phase.

II. EXPERIMENTAL

The spinel titanates $Mg_{1+x}Ti_{2-x}O_4$ were prepared by the solid reaction method [17–19]. The magnetic susceptibility was measured by using a Quantum Design MPMS magnetometer. The synchrotron x-ray diffraction was measured in $E=12.4$keV at Photon Factory BL-8B, and was analyzed by the RIETAN-FP program [20]. The powder neutron diffraction was measured at J-PARC BL21 NOVA. The sample was placed into a $V_{96.4}$-$Ni_{3.6}$ cell having an inner diameter of 6 mmϕ. The scattering intensity $S(Q)$ was examined by using Z-Rietveld and GSAS software [21]. The pair distribution function $G(r)$ was obtained by the Fourier transformation of $S(Q)$, and analyzed using the PDFgui program [22]. The x-ray absorption spectra were measured near the Ti K edge at Photon Factory BL-9C and 12C, and were examined by Athena and Artemis [23].

III. RESULTS AND DISCUSSION

We show the temperature dependence of the (8 0 0) Bragg peak, whose index is defined in the cubic phase, in the x-ray diffraction in $MgTi_2O_4$ in Fig.1(c). The (8 0 0) peak splits into two below ≈ 245K, and this splitting indicates the structural transition from the cubic phase ($a=b=c$) to the tetragonal phase ($a'\sqrt{2}=b'\sqrt{2}>c'$) upon cooling, as shown in Fig.1(d).

In order to clarify the Mg substitution effect on the structural phase transition in $Mg_{1+x}Ti_{2-x}O_4$, we display the (8 0 0) peak profiles for various x in Fig.1(e). The (8 0 0) peak merges for $x \geq 0.06$. The tetragonal phase completely collapses by substituting several percent of Mg ions, and the cubic phase is resurrected. The lattice constants (Fig.1(f)) were obtained by the Rietveld analyses. In this cubic phase ($x \geq 0.06$), the Bragg peak broadens slightly at the lower temperatures, indicating the growth of the short-range order of the tetragonal structure. The difference in full width at half maximum between 300 K and 20 K, as shown by the black circle in the inset of Fig.1(e), decreases on increasing x, and is hardly seen above $x = 0.25$.

To reveal the local structure, we measured the neutron diffraction. Figure 2(a) shows the neutron scattering intensity $S(Q)$ in $MgTi_2O_4$. As indicated by the asterisks in the inset of Fig.2(a), these reflections forbidden in the cubic phase are observed at 20 K, and indicate that the average symmetry changes into tetragonal $P4_12_12$ below T_c. The indices in $P4_12_12$ are shown in the inset. As shown in Fig.2(b), the PDF $G(r)$ is obtained by the Fourier transformation of $S(Q)$ for $Q = 0.9 \sim 40$ Å^{-1}. Figure 2(d) displays the $G(r)$ at 20 K, 300 K, and 450 K. As shown in Fig.2(c), the dip at $r = 2.1$ Å corresponds to the two-body correlation between the Ti and O ions, and the peak at $r = 3$ Å is ascribed to the Ti-Ti and the O-O atomic pair correlations. The PDF profile at 20 K can be reproduced by assuming the tetragonal symmetry of $P4_12_12$. Though the structural phase transition takes place at $T_c \approx 260$ K, no clear difference in the local structure is seen in the data at 20 K$\sim$450 K, indicating the local tetragonal structure even above T_c. As shown in Fig.2(e), we compared the simulation with the experimental result (circle) measured at 300 K. First, we assumed the cubic $Fd\bar{3}m$ and the atomic coordinates obtained by the Rietveld analysis. The black curve indicates the result obtained by adjusting the Debye-Waller factors. In the simulation on the assumption of the $Fd\bar{3}m$, the dip near $r = 2.1$ Å corresponding to the Ti-O pair appeared not to agree with the experimental result. This is because a large U value in the Debye-Waller factor is required to reproduce the broad peak due to the Ti-Ti and O-O atomic pair correlations in $r = 3$ Å, as listed in Tab.S1 in the supplemental material [19]. The sharp dip due to the Ti-O correlation in $r = 2.1$Å cannot be explained by this large U value. Next, we consider the tetragonal $P4_12_12$ [12]. The red curve indicates the analysis result obtained by allowing for the Ti, Mg, and O atomic displacements. Here, the direction of the Ti atomic displacement is restricted to the displacement direction obtained

by the Rietveld analysis of the neutron diffraction at 20 K. The simulation in $P4_12_12$ can reproduce the sharp dip in $r = 2.1$Å. Here, the value $R_w(P4_12_12) = 12.1\%$ is lower than that of $R_w(Fd\bar{3}m)$=14.9%. As listed in Tab.S1, two kinds of O sites (O(1) and O(2)) exist, and the U values of the O sites and the Ti site are reduced. The Ti-O(2) distance is also close to the Ti-O(1) distance ($r = 2.00 \sim 2.09$ Å). Thus, the dip in $r = 2.1$ Å becomes sharp. On the other hand, the peak in $r = 3$ Å is still broad, since there are several kinds of Ti-Ti distances ($r = 2.88 \sim 3.12$ Å) and O-O distances ($r = 2.68 \sim 3.31$ Å). Therefore, the local structure has a tetragonal symmetry of $P4_12_12$ even above T_c.

To estimate the correlation length of the tetragonal structure, the simulation was carried out on the basis of the experimental data in the r range between r_{max} and r_{max} - 10 Å as indicated by the arrows in Fig.2(b), and the boxcar refinement was applied [24, 25]. Here, only for $r_{max} = 10$ Å, the $G(r)$ in $r = 1.5 \sim 10$ Å was analyzed. Figure 2(f) shows the r_{max} dependence of the distance between the neighboring Ti ions. At 20K, three kinds of Ti-Ti distances remain up to $r_{max} = 50$ Å, and are nearly consistent with the Rietveld analysis obtained by Schmidt *et al.*, as indicated by the thick bars on the right ordinate [12]. These long, intermediate, and short Ti-Ti distances are ascribed to the two-in two-out configuration of the Ti displacement, as illustrated in Fig.1(b). At 300 K above T_c, three kinds of the Ti-Ti distances still exist. In r_{max}= 30 Å, the values of the Ti-Ti distances merge to ≈ 3 Å. Thus, the correlation length ξ of the tetragonal structure is estimated to be $\xi = 10$ Å. Here, this ξ is defined as the half of $r_{max} - 10$ Å, if the Ti-Ti distances merge in r_{max} within standard error.

Next, we measured the $G(r)$ at 20 K in $Mg_{1+x}Ti_{2-x}O_4$ ($x = 0 \sim 0.4$) in order to investigate the Mg substitution effect on the Ti-Ti correlation, as shown in Fig.3(a). The depth of the dip at $r = 2.1$ Å due to the Ti-O correlation decreases with increasing x. This dip structure is influenced by not only the Ti displacement but also the substitution of the Mg ions for the Ti ions, since the neutron scattering length of the Mg ions has the opposite sign compared to that of the Ti ions. As shown in Fig.3(b), we performed the PDF analysis at 20 K for $x = 0.125$. The black and red curves indicate the results calculated by assuming the $Fd\bar{3}m$ and the Ti, Mg, and O displacements in $P4_12_12$, respectively, as listed in Tab.S2 [19]. Since the sharp dip at $r = 2.1$Å in Fig.3(b) can be reproduced by the red curve, the short-range order of the tetragonal structure remains. Here, the $R_w(P4_12_12)$=10.0% is lower than $R_w(Fd\bar{3}m)$ =12.4%. Figure 3(c) shows the r_{max} dependence of the Ti-Ti distance.

Three kinds of Ti-Ti distances reflecting the two-in two-out type Ti atomic displacement still remain. The correlation length ξ of the tetragonal structure is estimated to be 10 Å in $x = 0.125$. The value of ξ is shortened with increasing x. For $x > 0.32$, the Ti-Ti distances merge to ≈ 3 Å in the whole r_{max} range. Thus, the fluctuation of the tetragonal structure remains below x=0.25$\sim$0.32.

In order to focus on the two-body correlation with the Ti ion, we measured the Ti K edge EXAFS at 20 K in $Mg_{1+x}Ti_{2-x}O_4$ ($x = 0 \sim 0.4$), as shown in Fig.3(d). The peaks around $r_{EXAFS} = 1.5$ Å and 2.5 Å correspond to the Ti-O and Ti-Ti atomic pair correlations, respectively. The shape of the peak due to the Ti-Ti correlation changes in $x = 0.25 \sim 0.32$. Figures 3(e) and (f) display the simulation at 20 K in $x = 0$ and 0.4, respectively. Here, we used the structural parameters obtained by the neutron PDF analysis, as listed in Tabs.S3 and S4 [19]. In $x = 0$, we can reproduce the overall feature of the two-peak structure due to the Ti-Ti correlation in $r_{EXAFS} = 2.1 \sim 2.5$ Å by assuming the $P4_12_12$. In $x = 0.4$, the simulation in $Fd\bar{3}m$ can reproduce the peak structure in this r_{EXAFS} range well. Thus, the short-range order of the tetragonal structure exists below $x = 0.25 \sim 0.32$. It is known that the peak position r_{EXAFS} obtained by the EXAFS deviates from the actual distance r of atomic pairs owing to the phase shift [26, 27]. In $x = 0$, for example, the actual Ti-O and Ti-Ti distances are $r = 2.01 \sim 2.11$ Åand $2.86 \sim 2.98$ Å, respectively.

On the basis of the obtained experiment results, we present the phase diagram in Fig.4(a). For $x > 0.06$, the structural transition temperature T_c drops to zero. Nevertheless, as displayed in Fig.4(c), the reduction of the magnetic susceptibility below T_c, which is defined as $|\chi(150\,\mathrm{K}) - \chi(260\,\mathrm{K})|$, is still discernible. The temperature T_{mag}, below which the magnetic susceptibility decreases, remains at $\approx$ 230K. This decrease of the magnetic susceptibility below x=0.25 was also reported in the previous studies [17, 18], and becomes unclear above x=0.29. In Fig.4(b), the correlation length ξ suggests that the nanoscale fluctuation of the tetragonal structure exists up to x=0.25$\sim$0.32 in the cubic phase at 20 K. This structural fluctuation is consistent with the decrease of the magnetic susceptibility below x=0.25. The local Ti dimer likely forms the spin-singlet pair, since the decrease of the intradimer Ti-Ti distance ($\Delta r \approx 0.1$ Å) is larger than that of the intradimer Cu-Cu distance ($\Delta r \approx 0.016$ Å) in $CuGeO_3$ [28]. The resistivity increases on lowering the temperature. Below x=0.06, the kink structure is seen at the structural transition temperature T_c [18]. Above x=0.06, the kink structure of the resistivity broadens with x. This behavior is in accord with the fact

that the correlation length of the tetragonal structure decreases with x.

In the structural transition to the tetragonal phase in $x = 0$, the Ti dimers are arranged along the c axis [12]. This structural transition relieves the frustration originating from the degeneracy of the Ti dimer formation [14, 15]. However, a tiny amount of Mg substitution causes the sudden collapse of the tetragonal phase, and the resurrection of the cubic phase. If the Ti^{3+} ions are substituted with the Mg^{2+} ions, the Ti ions, whose number is the same as that of the substituted Mg ions, have to have +4 charge. Since the substituted Mg ion and the Ti^{4+} ion do not have a valence electron, these ions do not form the dimer. Matteo *et al*. calculated the energy of the dimer formation, and found that the B3-type structure, in which one dimer is formed in one Ti tetrahedron, is favored [15], as shown in Fig.7 (Appendix). Taking into account the energy gain, since the Ti^{3+} ions tend to form the dimers of the B3-type structure, the substituted Mg ion and the Ti^{4+} ion make a nesting pair, as shown in Fig.8 (Appendix). At a finite temperature, the Ti^{4+} state can go away from the substituted Mg ion by the thermal excitation. The B3-type structures change into other B-type structures in the Ti tetrahedra around the path of the Ti^{4+} state. On the basis of the discussion of Matteo *et al*. [15], we assumed the energy difference between the B3-type structure and other B-type structure to be $\sim$2.5 meV per one Ti tetrahedron. If the Ti^{4+} state moves to the neighboring Ti tetrahedron or the neighboring Ti site, then two B3-type structures change. Thus, the Ti^{4+} state can go about five sites away from the substituted Mg ion near room temperature. In $Mg_{1+x}Ti_{2-x}O_4$, since the concentration of the substituted Mg ions is $x/2$ in the B site, the average distance between the substituted Mg ions is $\sim(2/x)^{1/3}$ sites. In low x, this distance is long, and the Ti^{4+}-Mg pair is isolated from other Ti^{4+}-Mg pairs. These Ti^{4+}-Mg pairs do not have a significant influence on the overall structure, and the tetragonal phase remains stable. In x=0.02$\sim$0.06, the distance between the substituted Mg ions is $(2/x)^{1/3}$ = 4.6$\sim$3.2 sites. The Ti^{4+} state can approach the Mg ions of other Ti^{4+}-Mg pairs near room temperature. As a result, the Ti^{4+}-Mg chain is linked with other Ti^{4+}-Mg chains, and the tetragonal phase becomes unstable in x=0.02$\sim$0.06. Such a phase transition driven by a tiny amount of substitution is characteristic of the ice-type materials [29].

The PDF analyses indicate the nanoscale fluctuation of the tetragonal structure. The correlation length ξ of this tetragonal structure approaches zero in $x = 0.25\sim0.32$, where the decrease of the magnetic susceptibility is still observed. Thus, in this x range, it is

suggested that the displacement-type ice state is created. As already discussed [15], the B-type structure is favored. In one Ti tetrahedron, there are two Ti ions forming one dimer, and the other two Ti ions. The occupied orbital of the latter Ti ion is directed towards the former Ti ion in the B3-type structure, and determines the position of the dimer in the neighboring Ti tetrahedron, as shown in Fig.7 (Appendix). As a result, the correlation length becomes the distance ($\sim$9Å) of about three Ti tetrahedra or three Ti sites in this x range.

IV. CONCLUSIONS

In the spinel titanates, the tetragonal phase collapses by substituting a tiny amount of Mg ions, and the cubic phase with the geometrical frustration is resurrected. We performed the nanoscale structural analyses and revealed a nanoscale structural fluctuation, in which the Ti displacement has the two-in two-out configuration, in the cubic phase.

Acknowledgments

The authors thank H. Kawamura, K. Uematsu, M. Isobe, K. Tomiyasu, and Y. Murakami for the valuable discussions. This work was supported in part, by the Asahi Glass Foundation, by a Grant-in-Aid for Scientific Research from the Japan Society for Promotion of Science (JSPS KAKENHI Grant Nos. JP16K13838, JP16H06015, and JP16H06114) and by JST PRESTO (No. JPMJPR16R2). The neutron scattering experiment was approved by the Neutron Science Proposal Review Committee of J-PARC MLF (Proposal Nos.2016A 0282 and 2017A0256) and supported by the Inter-University Research Program on Neutron Scattering of IMSS, KEK. The synchrotron radiation experiments were performed at BL-8B, 9C, and 12C of Photon Factory under the approval of the Photon Factory Program Advisory Committee (Proposal Nos.2015G709 and 2017G635). This work was done in part at the Center for Spintronics Research Network (CSRN), Graduate School of Engineering Science, Osaka University.

∗**Corresponding author**

hanasaki@phys.sci.osaka-u.ac.jp

---

[1] L. Pauling, *J. Am. Chem. Soc.* **57**, 2680 (1935).

[2] J. D. Benal and R. H. Fowler, *J. Chem. Phys.* **1**, 515 (1933).

[3] W. F. Giauque and M. F. Ashley, *Phys. Rev.* **43**, 81 (1933).

[4] P. W. Anderson, *Phys. Rev.* **102**, 1008 (1956).

[5] S. T. Bramwell and M. J. P. Gigras, *Science* **294**, 1495 (2001).

[6] P. G. Radaelli, Y. Horibe, M. J. Gutmann, H. Ishibashi, C. H. Chen, R. M. Ibberson, Y. Koyama, Y. -S. Hor, V. Kiryukhin, and S. -W. Cheong, *Nature (London)* **416**, 155 (2002).

[7] Y. Horibe, M. Shingu, K. Kurushima, H. Ishibashi, N. Ikeda, K. Kato, Y. Motome, N. Furukawa, S. Mori, and T. Katsufuji, *Phys. Rev. Lett.* **96**, 086406 (2006).

[8] Alexander J.Brown, Simon A. J. Kimber, and J. Paul Attfield, *Phys. Rev. Mater.* **1**, 052003 (2017).

[9] J. P. Attfield, *APL Materials* **3**, 041510 (2015).

[10] K. R. Knox, A. M. M. Abeykoon, H. Zheng, W. -G. Yin, A. M. Tsvelik, J. F. Mitchell, S. J. L. Billinge, and E. S. Bozin, *Phys. Rev. B* **88**, 174114 (2013)

[11] M. Isobe and Y. Ueda, *J. Phys. Soc. Jpn.* **71**, 1848 (2002).

[12] M. Schmidt, W. Ratcliff, P. G. Radaelli, K. Refson, N. M. Harrison, and S. -W. Cheong, *Phys. Rev. Lett.* **92**, 056402 (2004).

[13] D. I. Khomskii and T. Mizokawa, *Phys. Rev. Lett.* **94**, 156402 (2005).

[14] S. Di Matteo, G. Jackeli, C. Lacroix, and N. B. Perkins, *Phys. Rev. Lett.* **93**, 077208 (2004).

[15] S. Di Matteo, G. Jackeli, and N. B. Perkins, *Phys. Rev. B* **72**, 024431 (2005).

[16] Z. Hiroi, *Prog. Solid State Chem.* **43**, 47 (2015).

[17] M. Isobe and Y. Ueda, *J. Alloys Compd.* **383**, 85 (2004).

[18] H. D. Zhou and J. B. Goodenough, *Phys. Rev. B* **72**, 045118 (2005).

[19] See Supplemental Material.

[20] F. Izumi and K. Momma, *Solid State Phenom.* **130**, 15 (2007).

[21] R. Tomiyasu, M. Yonemura, T. Morishima, A. Hoshikawa, S. Torii, T. Ishigaki, and T.

Kamiyama, *J. Appl. Crystallogr.* **45**, 299 (2012).

[22] C. L. Farrow, P. Juhas, J. W. Liu, D. Bryndin, E. S. Bozin, J. Bloch, Th. Proffen, and S. J. L. Billinge, *J. Phys.: Condens. Matter* **19**, 335219 (2007).

[23] B. Ravel and M. Newville, *J. Synchrotron Rad.* **12**, 537 (2005).

[24] X. Qiu, Th. Proffen, J. F. Mitchell, and S. J. L. Billinge, *Phys. Rev. Lett.* **94**, 177203 (2005).

[25] K. Kodama, K. Ikeda, M. Isobe, H. Takeda, M. Itoh, Y. Ueda, S. Shamoto, and T. Otomo, *J. Phys. Soc. Jpn.* **85**, 094709 (2016).

[26] B. K. Teo, *EXAFS: Basic Principles and Data Analysis* (Springer, Berlin, 1986).

[27] S. Torigoe, Y. Ishimoto, Y. Aoishi, H. Murakawa, D. Matsumura, K. Yoshii, Y. Yoneda, Y. Nishihata, K. Kodama, K. Tomiyasu, K. Ikeda, H. Nakao, Y. Nogami, N. Ikeda, T. Otomo, and N. Hanasaki, *Phys. Rev. B* **93**, 085109 (2016).

[28] K. Hirota, D. E. Cox, J. E. Lorenzo, G. Shirane, J. M. Tranquada, M. Hase, K. Uchinokura, H. Kojima, Y. Shibuya, and I. Tanaka, *Phys. Rev. Lett.* **73**, 736 (1994).

[29] Jacob J. Shephard, Ben Slater, Peter Harvey, Martin Hart, Craig L. Bull, Steven T. Bramwell, and Christoph G. Salzmann, *Nat. Phys.* **14**, 569 (2018).

[30] C. Castelnovo, R. Moessner, and S. L. Sondhi, *Nature* **451**, 42 (2008).

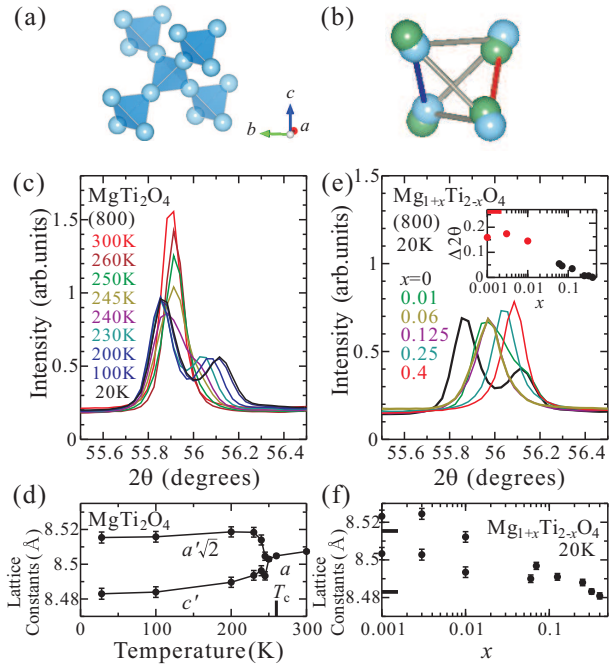

FIG. 1: (a) Schematic of the pyrochlore lattice. (b) Original positions of the atoms (blue spheres) and the positions of the displaced atoms (green spheres) in the two-in two-out type displacement. For clarity, the displacement is exaggerated. (c) (8 0 0) reflection in the x-ray diffraction in $MgTi_2O_4$. (d) Temperature dependence of the lattice constants. (e) (8 0 0) reflection at 20 K in $x = 0$, 0.01, 0.06, 0.125, 0.25, and 0.4. Inset: Difference in the angular position between the two peaks at 20 K (red) and the difference in the full width at half maximum between 300 K and 20 K (black), whose units are degrees. (f) x dependence of the lattice constants at 20 K. In the inset of (e) and in (f), the thick bars on the left ordinate indicate the values in $x = 0$.

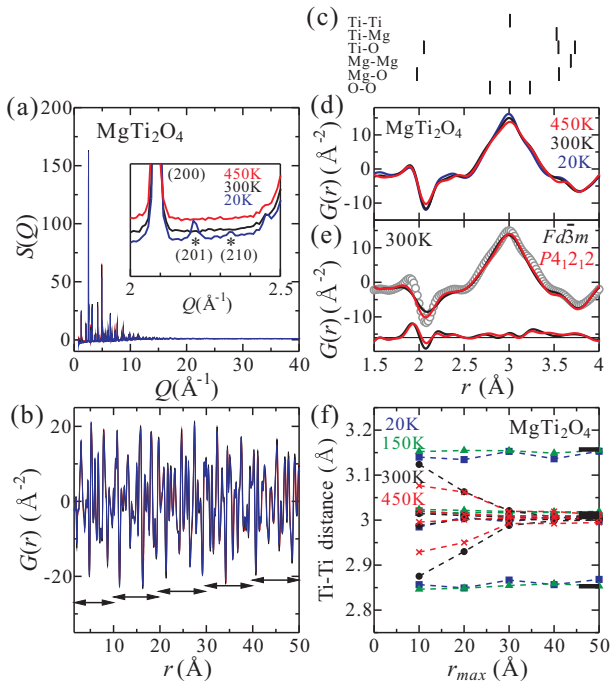

FIG. 2: (a) Observed powder neutron diffraction $S(Q)$ in $MgTi_2O_4$. Inset: Magnified view of the diffraction in $Q = 2 \sim 2.5\,\text{Å}^{-1}$. (b) Atomic pair distribution function (PDF) $G(r)$ in $r = 1.5 \sim 50\,\text{Å}$. The arrows indicate the ranges where the boxcar refinement was applied. (c) Barcodes indicating the distances of each atom pair under the assumption of cubic $Fd\bar{3}m$. (d) Experimental results of PDF in $r = 1.5 \sim 4\,\text{Å}$ at 450 K (red), 300 K (black), and 20 K (blue). (e) Observed PDF at 300 K (grey circle) and PDFs calculated by using the structural model; The assumption of $Fd\bar{3}m$ (black curve) and $P4_12_12$ (red curve). (f) Distance between the neighboring Ti ions as a function of the r_{max}, where the boxcar refinement was applied, at 450 K (red cross), 300 K (black circle), 150 K(green triangle), and 20 K (blue square). The thick bars on the right ordinate indicate the Ti-Ti distances obtained by the Rietveld analysis.

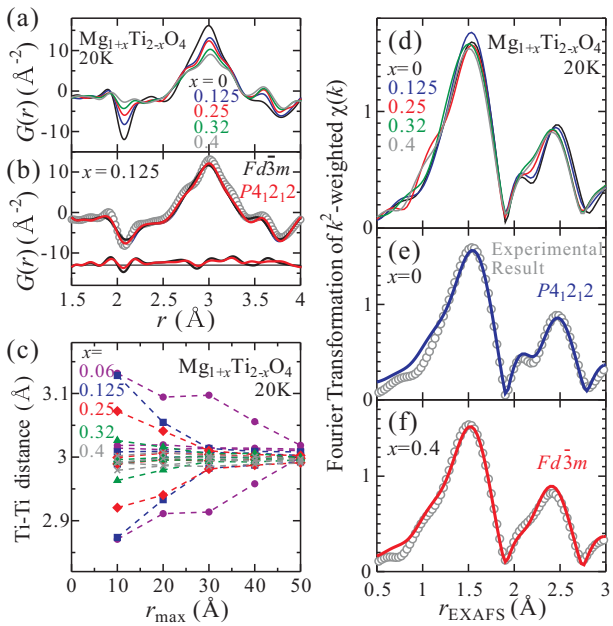

FIG. 3: (a) Observed neutron PDF $G(r)$ in $r = 1.5 \sim 4$ Å at 20 K in $x = 0$ (black), 0.125 (blue), 0.25 (red), 0.32 (green), and 0.4 (grey) of $Mg_{1+x}Ti_{2-x}O_4$. (b) Observed PDF at 20 K in $x = 0.125$ (grey circle) and the PDFs calculated by using the structural model; The assumption of $Fd\bar{3}m$ (black curve) and $P4_12_12$ (red curve). (c) Distance between the neighboring Ti ions as a function of the r_{max}, where the boxcar refinement was applied, in $x = 0.06$ (purple circle), 0.125 (blue square), 0.25 (red diamond), 0.32 (green triangle), and 0.4 (grey cross). (d) Radial distribution function in $r = 0.5 \sim 3$ Å obtained in the Ti K edge EXAFS in $x = 0$ (black), 0.125 (blue), 0.25 (red), 0.32 (green), and 0.4 (grey). (e) and (f) Experimental result (grey circle) at 20 K, and the simulations under the assumption of $P4_12_12$ (blue) and $Fd\bar{3}m$ (red) in $x = 0$ (e) and 0.4 (f), respectively.

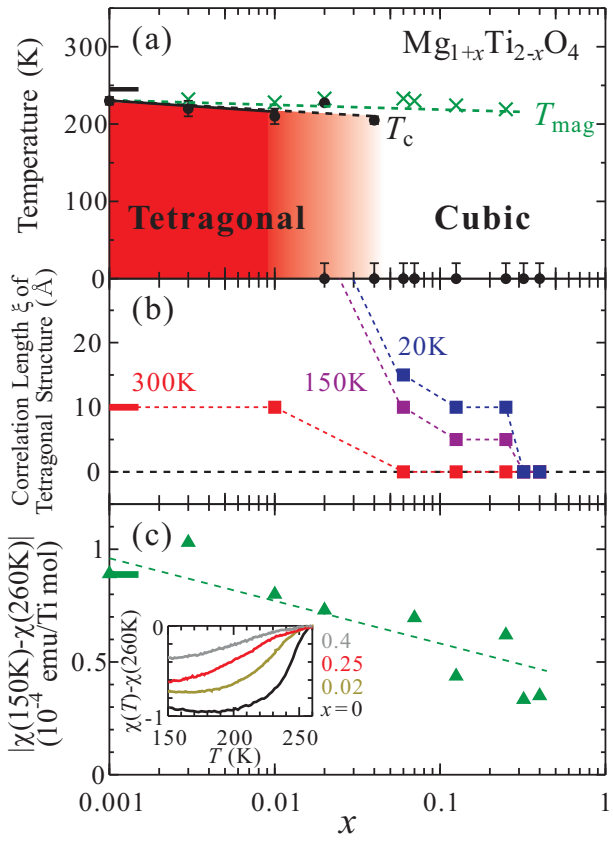

FIG. 4: (a) Phase diagram of the lattice structure and the magnetism in $Mg_{1+x}Ti_{2-x}O_4$. The black circles and the green crosses indicate the structural transition temperature (T_c) and the temperature (T_{mag}) at which the magnetic susceptibility decreases, respectively. (b) x dependence of the correlation length ξ of the tetragonal structure obtained by the PDF analyses at 20 K (blue), 150 K (purple), and 300 K (red). (c) Reduction of the magnetic susceptibility $|\chi(150\,\mathrm{K})-\chi(260\,\mathrm{K})|$. Inset: Temperature dependence of the magnetic susceptibility in which $\chi(260\,\mathrm{K})$ is subtracted from $\chi(T)$. The thick bars on the left ordinate in (a)$\sim$(c) indicate the values in $x=0$.

Appendix A: Disappearance of the tetragonal phase by the tiny amounts of Mg substitution.

In $MgTi_2O_4$, Schmidt *et al*. revealed the tetragonal structure releasing the frustration at low temperature [12]. Figure 5 illustrates the structure in this tetragonal phase, in which the spins in the Ti ions form the singlet dimers (the red lines). Matteo *et al*. suggested that this structure shown in Fig.5 has the lowest energy, taking into account the magnetoelastic effect [14, 15].

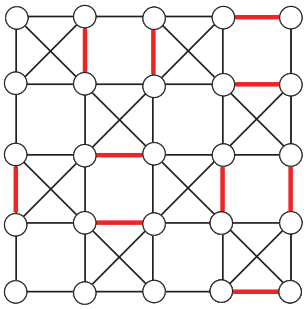

FIG. 5: Ti dimer configuration in the tetragonal phase, which is viewed from the c axis. The circles, the black lines, and the red lines indicate the Ti ions, the pyrochlore lattice, and the Ti dimers, respectively.

Though the frustration originally exists in the pyrochlore lattice, the title compound enters the tetragonal phase at lower temperatures. For the reader′s understanding of this situation, we show the example of the energy landscape in Fig.6. Here, the arrow indicates the position of the tetragonal phase.

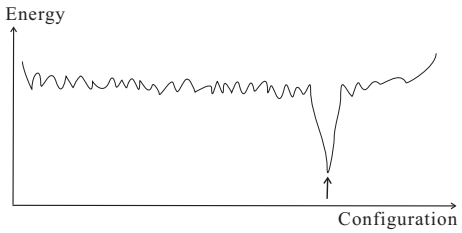

FIG. 6: Schematic picture of the energy landscape. The bottom abscissa means the configuration of the structure such as the dimer pattern. The arrow indicates the position of the tetragonal phase.

If the Ti^{3+} ions are substituted with the Mg^{2+} ions, the Ti ions, whose number is the same as that of the substituted Mg ions, have to have +4 charge. Since the substituted Mg ion and the Ti^{4+} ion do not have a valence electron, these ions do not form the dimer. The Mg substitution reduces the energy gain due to the dimerization. Thus, the energy of the tetragonal phase increases. If this tetragonal phase becomes unstable, the cubic phase is resurrected, leading to the frustration effect.

In the x range between x=0 and x=0.01$\sim$0.04, the phase transition temperature T_c decreases with x, as shown in Fig.4(a). This decrease of T_c is proportional to the decrease of the Ti dimer′s number due to the substitution of the Mg ions. Thus, the continuous decrease of T_c can be ascribed to the decrease of the Ti dimer′s number.

Matteo *et al*. calculated the energy in the A-type structure, in which two Ti dimers are formed in one Ti tetrahedron, the B-type structure, in which one Ti dimer is formed, and the C-type structure, in which no Ti dimer is formed, taking into account the magnetoelastic energy. They showed that the B-type structure has much lower energy as compared with the A-type and C-type structures. This fact suggests that the dimer pattern tends to follow the ice rule.

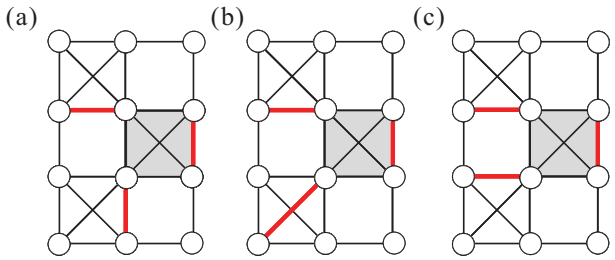

FIG. 7: (a) B1-type structure, (b) B2-type structure, and (c) B3-type structure in the grey Ti tetrahedron. The red lines indicate the Ti dimers.

Figure 7 illustrates the examples of the B-type structure. They discussed the difference in the energy between these B-type structures, and showed that the B3-type structure has lower energy than the B1-type and the B2-type structures [15]. On the basis of their discussion, we assumed this energy difference per one Ti tetrahedron to be $\sim$2.5meV ($\sim$20meV / 8 (tetrahedra/unit cell)). Since the Ti^{3+} ions form the dimers of the B3-type structure owing to the energy gain, the substituted Mg ion and the Ti^{4+} ion make a nesting pair, as illustrated in Fig.8 (a).

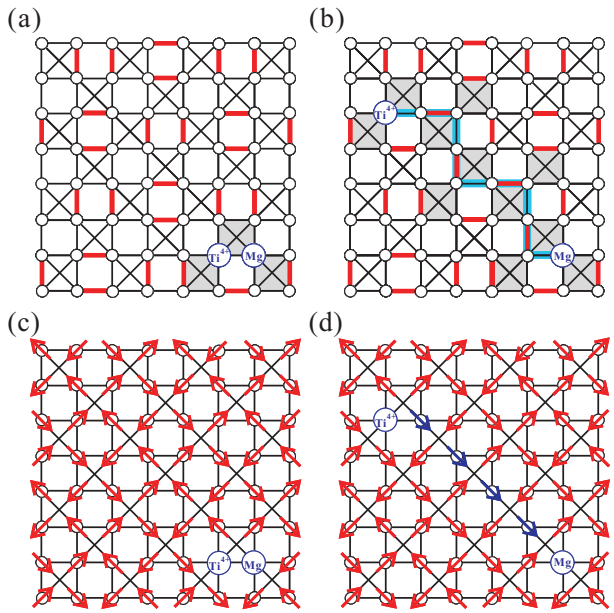

FIG. 8: Schematic picture of the pair of the substituted Mg ion and the Ti^{4+} ion. (a) Low-energy state : the Ti^{4+} ion and the Mg ion make a nesting pair. (b) Excited state : the Ti^{4+} state goes away from the Mg ion at a finite temperature. The blue curve indicates the path of the Ti^{4+} state. In the grey Ti tetrahedra, the Ti dimers do not form the B3-type structure. In (a) and (b), the red lines indicate the Ti^{3+} dimers. (c)(d) Picture in which the Ti displacements in the dimer formation are indicated by the arrows. (c) and (d) correspond to (a) and (b), respectively. In (d), the arrows are inverted by the movement of the Ti^{4+} state, as shown by blue arrows.

At a finite temperature, some B3-type structures can change into other B-type structures by the thermal excitation. As illustrated in Fig.8(b), the Ti^{4+} state can go away from the substituted Mg ion along the blue curve. Some B3-type structures change in the grey Ti tetrahedra around the blue curve. If the Ti^{4+} state moves to the neighboring Ti tetrahedron or the neighboring Ti site, one dimer is shifted, and then two B3-type structures change.

In Figs.8(c) and (d), the arrows indicate the Ti displacements due to the dimerization in (a) and (b), respectively. Here, the arrows on the Ti ions forming the dimer are directed inwards in the Ti tetrahedron. As shown by the blue arrows in Fig.8(d), the arrows are inverted along the path of the Ti^{4+} state. This inversion process of the arrows is similar to the process in the spin ice, in which the spins are inverted by the movement of the magnetic monopole [30].

If one assumes that the change of the B3-type structure needs the energy of ∼2.5meV per a Ti tetrahedron, about ten B3-type structures per a Ti^{4+}-Mg pair can change into other B-type structures near room temperature, since $(k_B\,260\mathrm{K})/2.5\mathrm{meV}\sim10$. If the Ti^{4+} state moves to the neighboring Ti tetrahedron or the neighboring Ti site, then two B3-type structures change. Thus, the Ti^{4+} state can go about five sites away from the substituted Mg ion.

Since the concentration of the substituted Mg ions is $x/2$ in the B site of $Mg_{1+x}Ti_{2-x}O_4$, the average distance between the substituted Mg ions is $\sim(2/x)^{1/3}$ sites. In low x, this distance is long, and the Ti^{4+}-Mg pair is isolated from other Ti^{4+}-Mg pairs. Thus, the Ti^{4+}-Mg pairs do not have any significant influence on the overall structure, and the tetragonal phase remains stable.

If the concentration of the substituted Mg ions increases, the Ti^{4+} state can approach the Mg ions of other Ti^{4+}-Mg pairs. In x=0.02∼0.06, the distance between the substituted Mg ions is $(2/x)^{1/3} = 4.6\sim3.2$ sites. Since the length of the Ti^{4+}-Mg chain is ∼5 sites near room temperature, the Ti^{4+}-Mg chain is linked with other Ti^{4+}-Mg chains, and the network of the Ti^{4+}-Mg chains is developed. As a result, the tetragonal phase becomes unstable, and changes into the cubic phase in x=0.02∼0.06.

It is known that the phase transition occurs by the impurity in ice [29]. By introducing a tiny amount of NH_4^+ and Cl^- ions, the ice II phase changes into the ice III phase having a large entropy owing to many kinds of the H_2O configuration. The frustration effect can be resurrected by doping, and such an unusual phenomenon is characteristic of the ice-type materials.